applied sciences

MDPI

Article

Impact Resisting Mechanisms of Shear-Critical Reinforced Concrete Beams Strengthened with High-Performance FRC

Carlos Zanuy * and Gonzalo S.D. Ulzurrun

Dept. Continuum Mechanics and Structures, Universidad Politécnica de Madrid, ETS Ingenieros de Caminos, 28040 Madrid, Spain; g.ulzurrun@upm.es

* Correspondence: carlos.zanuy@upm.es; Tel.: +34-910674154

Received: 2 April 2020; Accepted: 29 April 2020; Published: 1 May 2020

Abstract: Reinforced concrete (RC) structures typically present brittle failures by shear or punching under impact loading. High-performance fiber-reinforced concrete (HPFRC) has great potential due to its superior strength and energy absorption. The higher price and environmental cost of HPFRC compared to conventional RC can be effectively overcome by partially strengthening impact-sensitive RC members with HPFRC. To study the feasibility of this technique, HPFRC was applied as a tensile layer at the bottom of RC beams. Drop weight impact tests were carried out on beams with two values (35 and 55 mm) of HPFRC thickness, in addition to companion RC beams. Results show that the impact response can be divided into two stages: a first stage governed by local effects and shear plug formation at midspan, and a second stage governed by global beam behavior with formation of shear web cracks. A new resisting mechanism was observed for beams strengthened with HPFRC, as the strengthening layer worked similarly to a stress ribbon retaining the damaged RC and reducing fragmentation-induced debris. Such mechanism was fully achieved by the specimens with 35 mm HPFRC layer but was limited for the specimens with 55 mm HPFRC layer due to impact-induced interface debonding.

Keywords: impact testing; dynamic strength; HPFRC; strengthening

1. Introduction

Concrete structures might be subjected to low to heavy impacts during their service life. Either accidental (rock falls, tornado-debris) or human-induced (terrorist attacks) impact events can produce severe damage or even failure of concrete structures if the impact scenario has not been addressed in the design stage. As the concern of impact hazards has increased in recent years, the capacity of many existing concrete structures which were not designed against impacts is under discussion. In such situations, strengthening or retrofitting structural concrete members can be required [1–3].

It has been extensively reported that concrete structures subjected to impact exhibit a high sensitivity to develop brittle failures by shear or punching before yielding to longitudinal reinforcement, even in cases of structures designed to show a ductile response under quasi-static loading [4–7]. The differences between impact and quasi-static behavior are mainly due to three factors [8–10]: (a) inertia forces under dynamic loading lead to a time-dependent distribution of sectional forces different from the one under quasi-static loading; (b) material properties of concrete and steel are affected by the strain rate; (c) impulsive loading and wave propagation produce local damage near the impact zone. Due to the former factors, low energy-absorbing shear failures become dominant for reinforced concrete (RC) beams. In addition, spalling of concrete cover and fragmentation can

produce debris which can potentially damage goods or persons under the impacted structure. In order to improve the deformation capacity against impacts and avoid shear failures, different measures have been researched. On the one hand, external sand cushions or other protecting layers can be used to reduce the impact that reaches the structure [11]. On the other hand, the performance of RC can be enhanced with the use of fiber reinforcement. Ulzurrun and Zanuy [12] showed that steel-fiber reinforced concrete (SFRC) can improve the integrity and energy absorption capacity of shear-critical RC beams subjected to moderate-velocity impacts: A 0.5% volumetric amount of deformed or straight steel fibers significantly reduced fragmentation, increased energy absorption, and avoided shear failure in case of straight fibers, while a 1.0% fiber amount was able to avoid diagonal cracking failures and prevent flying fragments for both fiber types. Hrynyk and Vecchio [4] needed a 1.5% content of hook-end fibers to avoid punching failure of impact-loaded RC slabs with failure controlled by flexure under quasi-static loading; failure was by punching under impact with smaller fiber contents. The fiber geometry (and not only the amount) can play a significant role in impact regime, as the dynamic properties of SFRC depend on the rate sensitivity of the pull-out mechanisms mobilized during crack formation and propagation. Thus, Ulzurrun and Zanuy [13] concluded that short straight fibers are more efficient than hook-end fibers in dynamic regime because of their higher ability to develop full pull-out without brittle fiber rupture. In addition, the rate sensitivity of tensile properties of SFRC decreases as the fiber content increases [14,15]. Synthetic fibers have also shown to perform satisfactorily under high strain rates [16], and the combination of steel and synthetic fibers can contribute to reducing local damages and enhancing energy absorption under drop-weight testing [17].

Due to the significance of crack bridging and energy absorption capacity to prevent brittle failures, the design of impact-resisting structures seems an attractive field for the application of high-performance fiber-reinforced concretes. Such materials present high compressive strength and significant energy-absorption capacity in tension. Among them, a differentiation between high-performance fiber-reinforced cement composites (HPFRCC) and ultra-high performance fiber-reinforced concrete (UHPFRC) has been established as a function of compressive strength (a limit of 120–150 MPa is used by different standards [18–20]) and other properties. The tensile capacity of high-performance materials is achieved by two behavioral stages: pre-peak strain-hardening and post-peak softening. The strain-hardening stage is achieved by multiple microcracking before macrocracking localization [21] and is responsible for higher energy absorption than conventional SFRC, which only has post-peak softening.

A satisfactory impact response has been observed for reinforced beams when the conventional concrete is replaced by a high-performance material (R-HPFRCC of R-UHPFRC). Zanuy and Ulzurrun [22] compared conventional RC beams without stirrups to analogous R-HPFRCC specimens with 1.6% short steel fibers by volume; while the former failed by shear upon a single impact, the latter were able to resist five impacts with plastic hinge formation at the midspan and without shear cracking at the webs. Yoo et al. [23] showed that R-UHPFRC (2% short steel fibers) beams without stirrups were able to resist a number of subsequent impacts showing a crack pattern with multiple very thin flexural cracks. Othman and Marzouk [24] subjected R-UHPFRC plates to subsequent drop weight impacts, demonstrating that failure changed from punching after three impacts for 0% fiber content to flexure after 7, 9, and 18 impacts for 1%, 2%, and 3% content of short steel fibers, respectively.

Nevertheless, a massive use of high-performance materials in the form of R-HPFRCC or R-UHPFRC members presents the disadvantage of high cost (mainly due to the high amount of fibers, typically from 2% to 6% [21,25]). In addition, it is not a plausible solution for existing structures needing retrofitting. Rather, a more local application of the high-performance material as a strengthening layer can be a solution for impact-critical RC members. Such a configuration has shown to be efficient for rehabilitation or new construction of bridges [26], where researchers [27,28] have demonstrated that a UHPFRC layer not only contributes to the bending capacity but also to the shear strength of the composite member [29].

The application of HPFRCC or UHPFRC to dynamic scenarios can be favored by the positive strain-rate influence on the material properties, as other studies [14,30–34] have concluded that the tensile properties (peak strength, strain-hardening stage, and fracture energy) are kept in the high strain-rate domain (1–100 s^{-1}). The rate sensitivity of UHPFRC in bending has also been verified in impact tests [35,36]. At the structural level, to the authors' knowledge, only Habel and Gauvreau [1] have carried out impact testing on composite UHPFRC-RC slab strips. They studied two configurations with the UHPFRC layer on the compressive and tensile sides of the specimens, respectively. For the specimens with the UHPFRC on the compressive part, the strengthening layer provided good protection against crushing and spalling on the impact zone, but such a configuration did not take advantage of the most remarkable properties of the strengthening material (i.e., strain-hardening and crack-bridging in tension). For the specimens with the UHPFRC on the tensile part, the cantilever test configuration and the limited measuring equipment were insufficient to fully explore the impact response of the UHPFRC-RC system.

In the present paper, the impact performance of shear-critical RC beams strengthened with a thin layer of high-performance fiber-reinforced concrete on the tensile part is studied. Strengthening solutions are necessary for existing structures because even RC members designed to develop a ductile flexural failure mode under quasi-static loading might have shear failures under impact loads [4–7]. The structural configuration studied in this paper is intended to utilize the superior strength and energy absorption capacity in tension of the strengthening material. By means of the localized application of the strengthening layer at the tensile side, a solution is achieved with smaller costs than those requiring massive material use like R-HPFRCC or R-UHPFRC (which in addition are not applicable to strengthen existing structures). Furthermore, the strengthening material has a more moderate fiber amount included (2% by volume, still able to achieve strain-hardening in tension) than common UHPFRC, thereby contributing to moderate economic and environmental impact. Drop-weight impact tests were carried out on strengthened beam specimens without stirrups. Two configurations were studied for the strengthening layer, as well as a reference series of conventional RC beams tested for comparison.

2. Experimental Methodology

2.1. Test Configuration and Set-Up

Drop-weight testing has shown to be an effective experimental configuration to investigate the response of concrete structures under impact at a laboratory [37]. In the present research, three series of beam specimens were tested with the drop-weight testing machine of the Laboratory of Structures at the Technical University of Madrid (UPM, Spain). The experimental campaign is intended to evaluate the possibilities of a high energy-absorbing strengthening layer for RC beams without stirrups (i.e., with a high tendency to present brittle shear failure, local damage, and fragmentation under impact events).

Tested specimens were 2000 mm long and had a rectangular cross-section of 125 mm (width) × 250 mm (height). The longitudinal reinforcement consisted of 2 steel bars of 16 mm diameter at the top and bottom of the beams (ϱ = 1.6%). A clear cover of 50 mm was considered between the bars and the beam edges in order to allow the installation of a strengthening layer on the tensile side. The test set-up and cross-sectional configuration of each series are plotted in Figure 1. No shear reinforcement was installed, except for two stirrups of 8 mm diameter on the supports to enhance anchorage of longitudinal bars. Reference series RC-U0 consisted of conventional RC beams, while series RC-U35 and RC-U55 included a 35- and 50-mm thick tensile layer of high-performance fiber-reinforced concrete, respectively, to simulate rehabilitation or strengthening of reference series. The reinforcement layout of reference series RC-U0 is a typical one of shear-critical RC members [12], which can be designed according to the most current shear models [38]. In series RC-U55, the interface between the conventional concrete and the strengthening material was placed at the level of the

longitudinal steel reinforcement. Two specimens were tested for each configuration (i.e., a total of six impacts tests was completed).

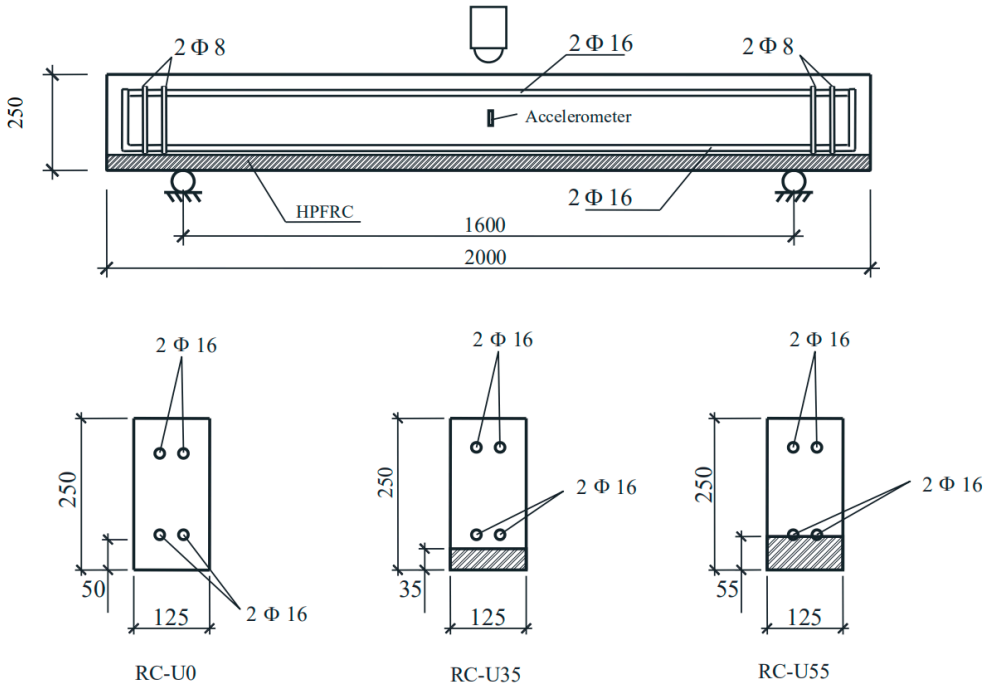

Figure 1. Test set-up and geometry of specimens (dimensions in mm).

Impact tests were carried out with a three-point bending scheme, with a span length of 1600 mm between supports, as plotted in Figure 1. A steel mass of 200 kg was freely dropped to the top side of the midspan of specimens from a height of 1.75 m (impact velocity = 5.9 m/s). The striking end of the projectile and the supports were cylindrical with 29 mm radius. At both supports, two steel yokes prevented uplift of the specimens. The impact load and reaction forces were measured with HBM piezoelectric force washers suited for highly dynamic solicitations with a sensitivity of 4.3 pC/N (CFW-700 and CFW-190, respectively). The vertical acceleration at the specimens' midspan was measured with a PCB piezoelectric accelerometer of 5 mV/g sensitivity, placed at mid-height of the cross-section (125 mm from bottom). The midspan acceleration is a representative measurement of the beam response and allows integration to achieve midspan displacements as explained in Section 2.3. The measurements were taken at a sampling rate of 40 kHz with an HBM expressoDAQ module. A comprehensive description of the testing machine is reported elsewhere [12,13]. An overview of the impact test configuration in the laboratory is given in Figure 2. It is noted that beam dimensions and test configuration are identical to those used in previous research of reinforced SFRC beams [12], except for the concrete cover, which was 40 mm, so that a comparative database including different cross-sectional schemes can be available for researchers.

Figure 2. Overview of an impact test at Technical University of Madrid, Spain (UPM).

2.2. Specimens' Preparation and Material Characterization

The beam specimens were manufactured at the Laboratory of Structures at UPM. In order to ease the placement of the strengthening layer, the beams were manufactured upside down. The conventional concrete was supplied by a local contractor. For series RC-U35 and RC-U55, the thickness corresponding to the strengthening layer was left empty during concreting of the conventional concrete (i.e., no demolition works of the concrete cover were carried out). The upper surface of the RC layer was prepared with a slight treatment consisting of wire-brushing and water-pressure cleaning. Though a more exhaustive surface treatment (e.g., sand blasting) is typically recommended [26], it has been preferred to keep a less demanding interface closer to real conditions of structures strengthened on the bottom side. An additional method for application of bottom strengthening is by bonding a prefabricated laminate with epoxy adhesive [39,40]. Before pouring the strengthening material, the surface was washed again and kept moist. Fabrication and pouring of the strengthening material was carried out 15 months after manufacturing the RC.

The conventional concrete was designed for a characteristic strength of 30 MPa. The maximum aggregate size was 12 mm, the content of Portland cement I 42.5 R was 350 kg/m^3 and the water/cement ratio was 0.5. The average cylinder (150 mm × 300 mm) compressive strength at 28 days was 38.1 MPa. At testing age, the average cylinder (150 × 300 mm) compressive and indirect (Brazilian) tensile strength were 40.8 MPa and 2.3 MPa, respectively. The reinforcing steel bars had a characteristic yield and ultimate strength of 500 MPa and 575 MPa, respectively.

The strengthening material consisted of a dry mortar premix of compact-reinforced concrete (CRC kindly supplied by Hi-Con A/S, Hjallerup, Denmark), which was mixed with water and fibers following the supplier's instructions. A 2% volumetric content of short steel fibers (l_f = 12.5 mm,

d_f = 0.3 mm, f_y = 2950 MPa) was used. The flow diameter in the slump flow test was larger than 550 mm, which allows classifying the mixture as self-compacting according to the French Association for Civil Engineering, AFGC [19]. The beams were tested 2 months after strengthening. The average cubic (150 mm) compressive strength of the strengthening material was 126.4 MPa and 135.4 MPa at 28 days and testing age, respectively. Flexural-tensile tests were carried out on un-notched and notched prismatic (100 × 100 × 500 mm, with span length between supports of 420 mm in all cases) samples at the age of beam tests. Un-notched samples were tested in a 4-point bending scheme. The results are represented in Figure 3a in terms of load-midspan deflection and equivalent bending stress-midspan deflection diagrams. A detail of the pre-peak stage is also plotted. Very thin cracks at a separation of 12–16 mm were observed in the central part of the specimens before localization of a macro-crack under peak strength, thereby showing the strain-hardening stage. The equivalent bending strength was 14.1 MPa on average. Notched samples were tested in a 3-point bending configuration with a 5 mm depth notch at midspan. Load-crack width results are plotted in Figure 3b. The average tensile properties of the strengthening material were estimated from inverse analysis of flexural tests according to López and colleagues [41] and the results are listed in Table 1. The free shrinkage strain was also measured in 2 cylinders of 150 × 300 mm, showing an average strain of -180×10^{-6} from manufacturing to testing age. Hereafter, the strengthening material will be referred to as high-performance fiber-reinforced concrete (HPFRC), as it has high compressive strength and tensile strain-hardening.

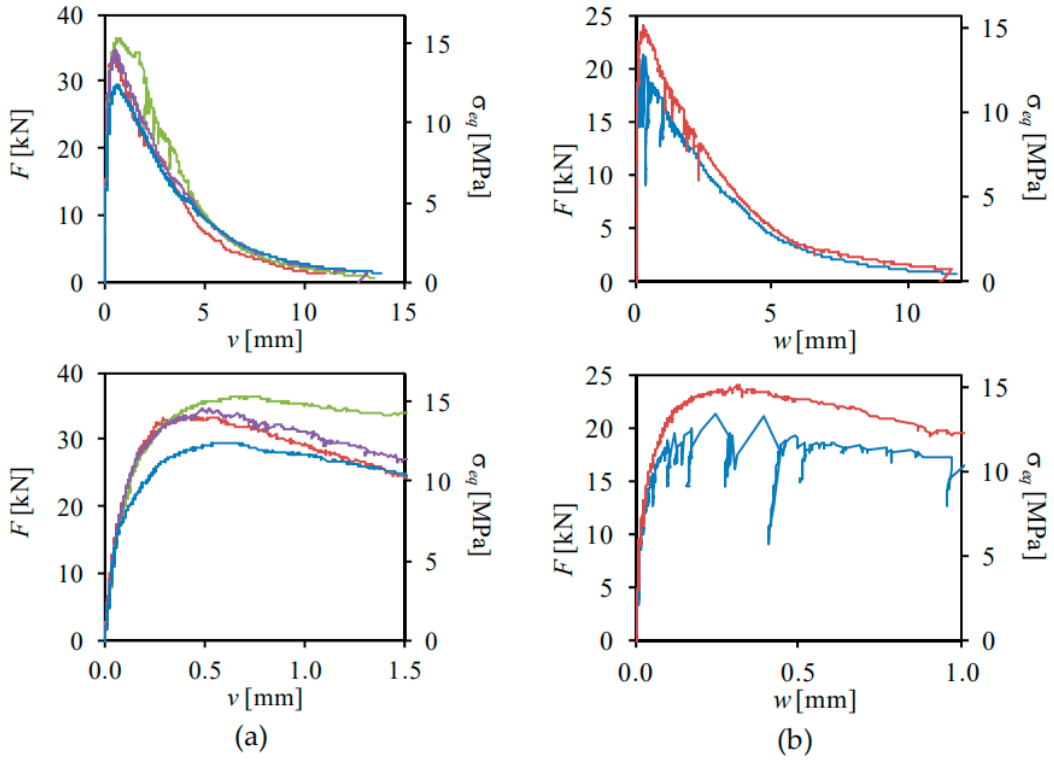

Figure 3. Flexural-tensile tests of high-performance fiber-reinforced concrete (HPFRC) prisms: (**a**) un-notched specimens, 4-point bending; (**b**) notched specimens, 3-point bending.

Table 1. Material properties of the strengthening material1.

	f_{CU} (MPa)	E_{CU} (MPa)	σ_{cc} (MPa)	ε_{pc} (-)	σ_{pc} (MPa)	G_F (kN/m)
Average	135.4	53382	4.6	0.0022	6.2	9.9
CoV	0.02	0.03	0.07	0.32	0.11	0.15

[1] f_{CU}: compressive strength, E_{CU}: elastic modulus, σ_{cc}: matrix cracking strength, ε_{pc}: hardening strain at peak strength, σ_{pc}: peak strength, G_F: fracture energy, CoV: coefficient of variation.

2.3. Test Results

The impact solicitation of the specimens can be understood from the measurements taken by the load cells and the accelerometer. Exemplarily, the records of test RC-U0-IMP-1 are represented in Figure 4. Reactions measured at both supports are symmetrical in all tests, whereby the total reaction is represented. Both impact force and total reaction had a two-stage shape over time, first with a high-frequency peak followed by a second stage with a smaller frequency. The peak of the impact force was higher than that of the total reaction. A time gap of 2–3 ms was observed between the beginning of the impact event and the activation of the support reactions due to the time required for the wave propagation from the midspan to the supports. The difference between impact force and total reaction makes it clear that inertia forces developed, which can be verified by the acceleration measured at midspan (Figure 4). Though strains were not measured in the present experimental campaign, previous tests under similar conditions have shown that strain rates can be in the range of 1–30 s^{-1} [12].

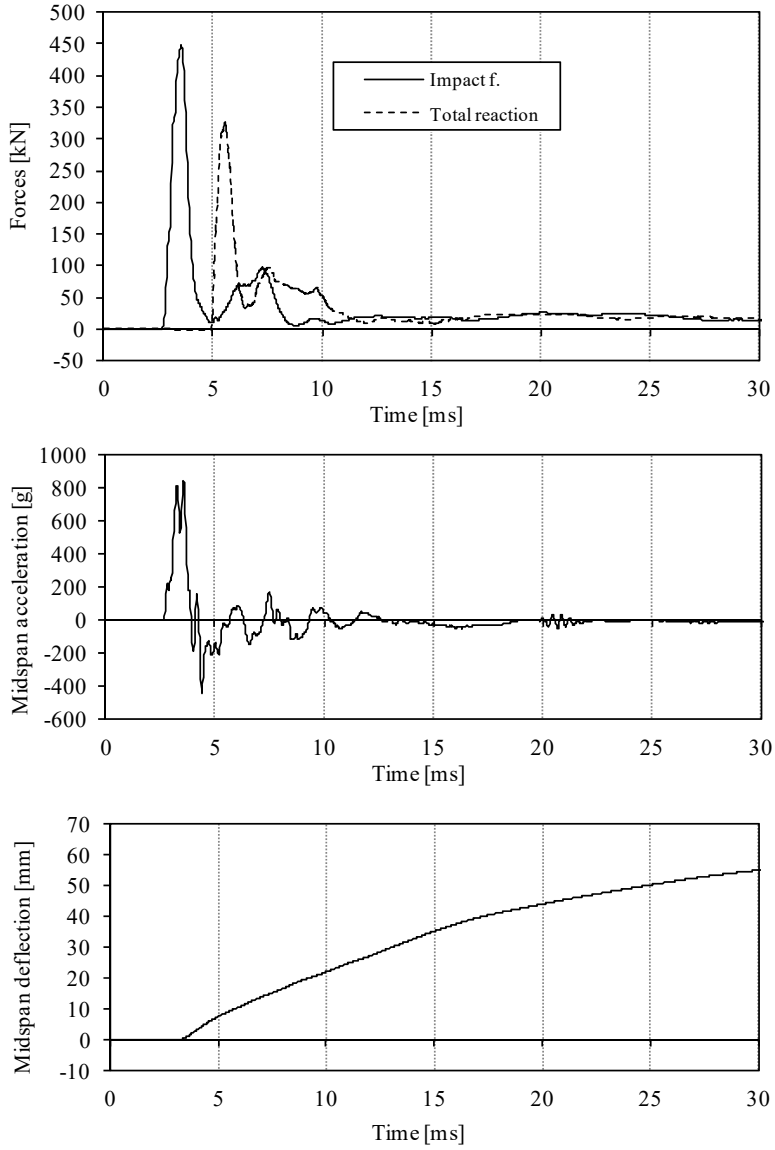

Figure 4. Dynamic measurements and midspan displacement over time for test RC-U0-IMP-1.

Pictures of deformed shapes and failure patterns of all tested specimens are given in Figure 5, while the main test results are summarized in Table 2. The strength (R_{max}) has been taken as the peak of

the total reaction at both supports. It has to be noted that such a value differs from the maximum impact load due to the effect of inertia forces. The total reaction has to be used as a strength indicator rather than the impact load unless the effect of inertia forces is removed from the impact load, which in turn is equivalent to the total reaction [12,42,43]. Total reaction-midspan deflection diagrams are represented in Figure 6 for all tested series. The midspan deflection was calculated by double integration of the measured acceleration, in agreement with previous research [12,43–45]. As observed in Figure 6, there is a shift of the origin of total reaction-deflection diagrams due to the fact that a deflection at the midspan already developed when the impact effect reached the supports (refer to Figure 4 as well).

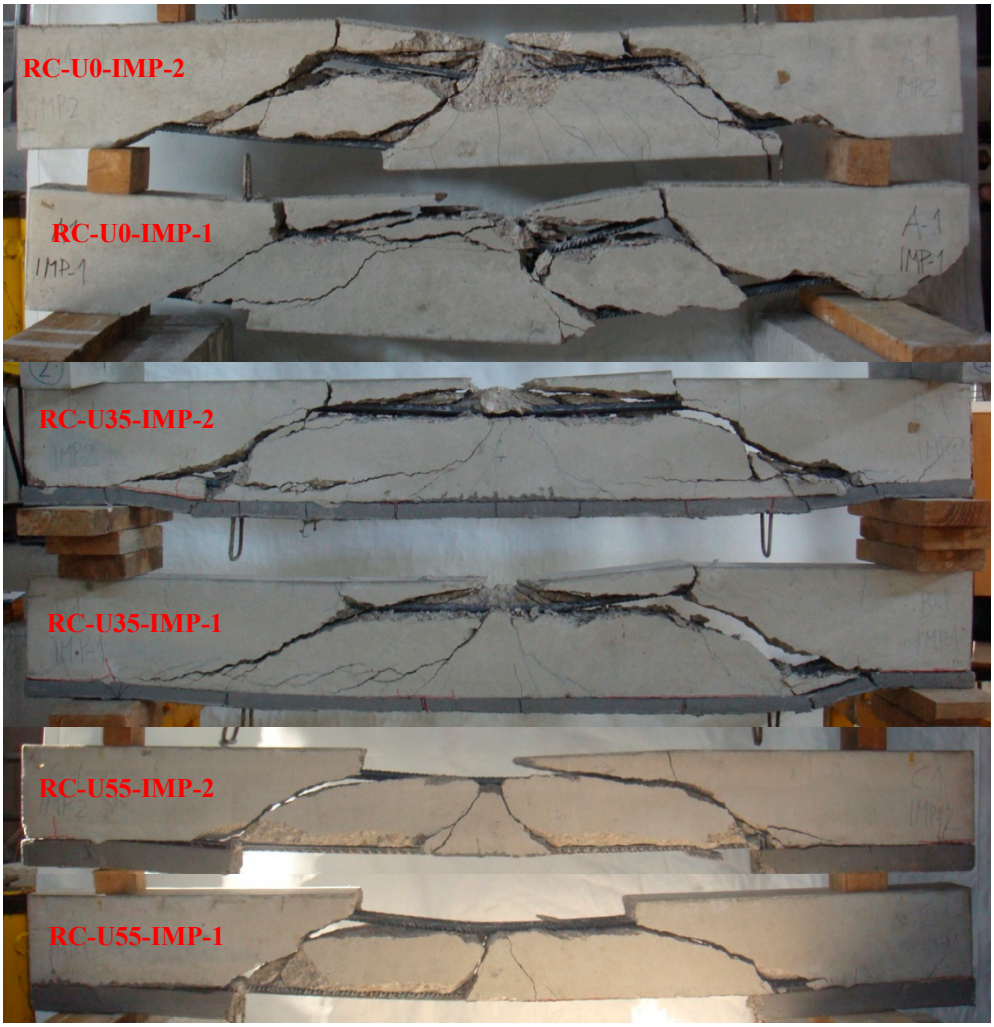

Figure 5. Crack pattern diagrams of tested specimens.

Table 2. Summary of test results[1].

Series	Test ID	R_{max} (kN)	v_{max} (mm)	v_{res} (mm)	E_1 (kJ)	E_2 (kJ)
RC-U0	RC-U0-IMP-1	325.6	59.7	59.7	0.82	0.75
	RC-U0-IMP-2	209.5	67.8	67.8	1.32	0.46
RC-U35	RC-U35-IMP-1	297.2	37.5	7.5	1.08	0.93
	RC-U35-IMP-2	278.6	43.7	28.3	1.02	1.64
RC-U55	RC-U55-IMP-1	263.8	38.7	38.7	1.04	1.57
	RC-U55-IMP-2	275.2	39.3	39.3	0.88	1.69

[1] R_{max}: peak total reaction, v_{max}: peak midspan deflection, v_{res}: residual midspan deflection, E_1 and E_2: energy absorbed in the first and second stage of test, respectively.

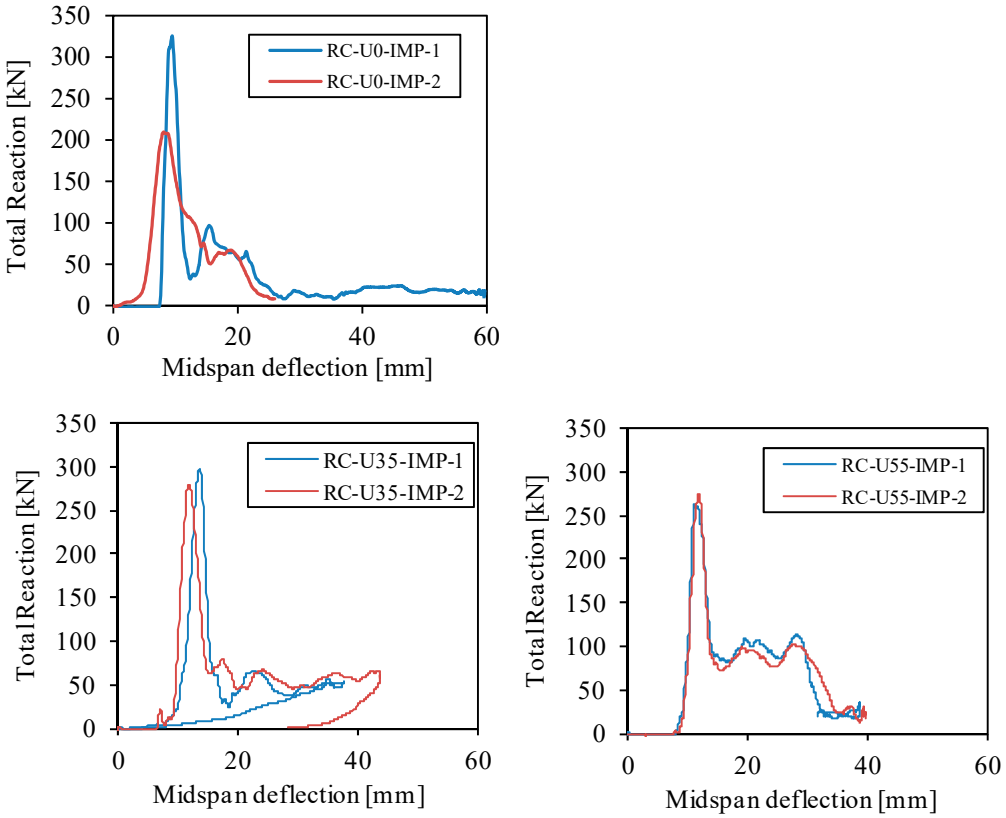

Figure 6. Load-midspan deflection diagrams of tested specimens.

From the crack patterns at failure (Figure 5), it is clear that all beam specimens presented extensive shear cracking. The conventional RC beams (series RC-U0) failed by shear with various diagonal cracks, multiple fragmentation, and cover spalling, whose induced debris is one the most undesirable hazards for humans and goods under structures subjected to impacts. The crack patterns of the beams strengthened with a HPFRC layer showed the development of two types of shear cracks (Figure 5): on the one hand, two diagonal cracks with an inclination of 45° or higher forming a shear plug at the midspan; on the other hand, two diagonal cracks in both shear spans with a shape similar to shear-flexure cracks typically developed in quasi-static tests of RC [12]. Yi et al. [8] classified the former crack categories as type I (shear plug) and type II (diagonal cracks at shear spans), as schematized in Figure 7b. The most interesting difference between the failure pattern of the two strengthened series can be observed at the HPFRC layer: in series RC-U55, debonding occurred at the interface between HPFRC and RC, and the HPFRC between the two type II cracks was split out; meanwhile, the HPFRC in series RC-U35 was able to stay in contact with the RC and to develop a resisting mechanism similar to a stress ribbon able to retain the damaged RC part. This last mechanism can be very interesting for real structures, as it has the potential to protect humans and goods below the structure.

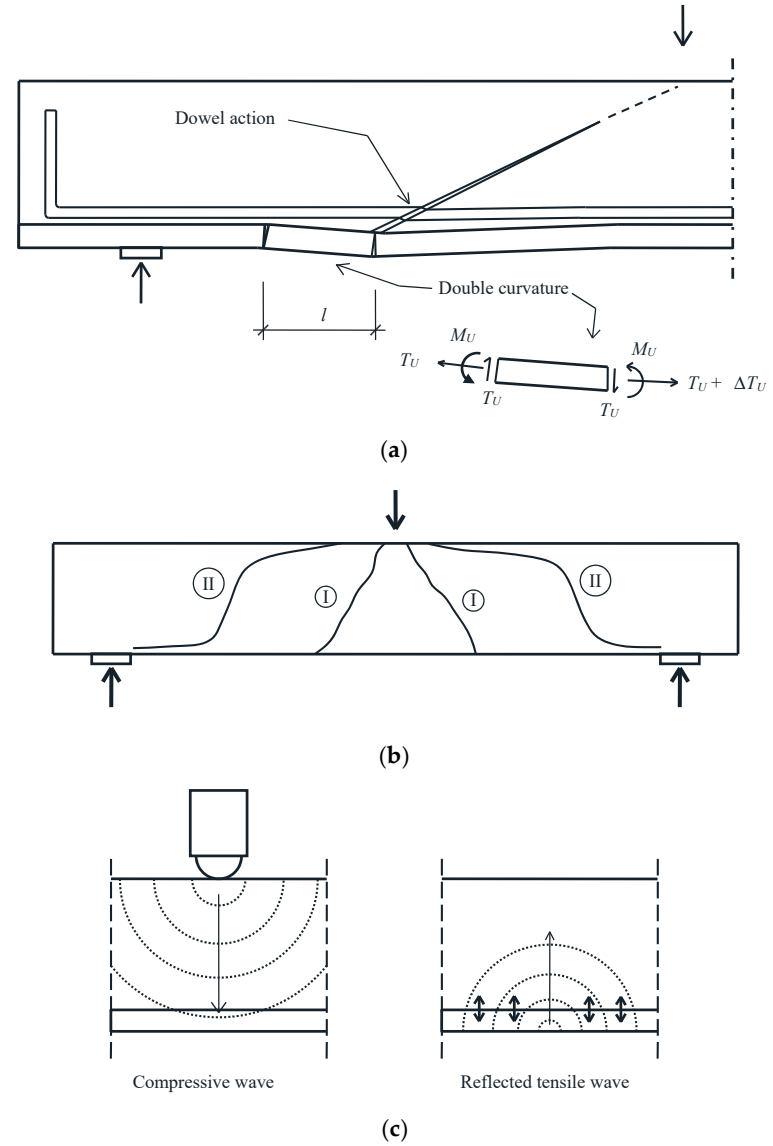

Figure 7. Shear resisting mechanisms. (**a**) Contribution of the HPFRC by bending in double curvature; (**b**) types of shear cracks in impact tests; (**c**) interface debonding due to reflected impact wave.

The shape of the load-deflection diagrams of Figure 6 can be useful to understand the different behavior of tested series. Such diagrams can be divided into two stages: first, a high-peak triangular stage and a secondary post-peak stage. While the amplitude of the first peak provides the load carrying capacity, the second stage gives information on the post-peak deformation and energy absorption capacity after first stage, which is governed by the HPFRC strengthening layer. Even though the average values of the first peak were rather similar for the three series (except for some scatter within series RC-U0; refer to Section 3, where the differences are analyzed), significant differences can be observed in the second stage. For RC-U0 series, the second stage was rather small, which explains the almost negligible post-peak capacity, in agreement with the observed failure mode. In contrast, RC-U35 and RC-U55 series showed a longer second stage, but a remarkable difference can be observed at the end of this second stage: in the two tests of RC-U35 series, a significant part of the deflection was recovered as the load released, which reminds the unloading stage of a specimen under quasi-static loading. The descending branch can be understood as a sign of the integrity of the HPFRC layer which explains the resisting mechanism achieved by the HPFRC layer in RC-U35 series. In contrast,

the former descending branch cannot be observed in the tests of RC-U55 series, where the HPFRC was debonded by the impact.

3. Results and Discussion

3.1. Phenomenology of Resisting Mechanisms

The brittleness and high tendency to develop shear cracking and fragmentation of RC beams under impact loading were confirmed by the results of RC-U0 series. Test results indicate that the impact response of strengthened specimens mobilized more complex resisting mechanisms than those reported for quasi-static loading scenarios. Previous researchers [46] explained that the contribution of the HPFRC layer to the shear capacity under quasi-static loading can be due, on the one hand, to the increase of the shear strength of the RC layer and, on the other hand, to additional shear resisting mechanism. The former can be explained by the capacity of the HPFRC layer to control the width of the critical shear crack, thereby increasing aggregate interlocking, as well as enlarging the compression zone depth, which in turn increases its capacity to carry shear stresses. The additional contribution was assigned by Noshiravani and Brühwiler [29] to the capacity of the strengthening layer for bending in double curvature along the interlayer debonding zone, as depicted in Figure 7a. It has to be noted that critical shear cracks under quasi-static loading can be assimilated to previously defined type II cracks.

The present experimental results show that two types of shear cracks (I and II as defined previously, see Figure 7b) developed. Type I cracks opened immediately upon impact as a local effect, while type II cracks were due to flexure-shear interaction at the webs produced by inertia forces, as similarly reported by previous researchers [6,8,47]. From the video records of completed tests, the sequence of crack development and activation of internal forces are as follows: The impact load is firstly resisted by inertia forces in the midspan, before the activation of reaction forces. At this stage, the midspan zone is highly stressed and type I cracks develop. In the second stage, when reaction forces are activated and the impact force is cancelled, inertia forces are fully equilibrated by the reaction forces. Shear forces and bending moments in the second stage are responsible for type II cracks. Due to the similar crack patterns of all tested specimens, it seems that the formation of type I and II cracks was not affected by the presence of a HPFRC layer. Rather, the contribution of the stress ribbon mechanism of the HPFRC layer was activated upon the formation of such cracks and responsible for the retention of the damaged RC part of the beams and control of fragmentation. The crack pattern of RC-U35 series indicates that the full tensile capacity of the HPFRC was utilized by the stress ribbon mechanism, as the HPFRC layer shows visible macrocracks at an average distance of 180 mm to each other (Figure 5). In RC-U35 series, the stress ribbon mechanism was able to bridge the damaged zone between the two type II cracks. The full utilization of the tensile capacity of the HPFRC confirms conclusions made in previous research (see [14,30–34]) on the positive strain-rate influence on the tensile properties of HPFRC in the impact domain. Such strain rate has been in the range of 1–30 s^{-1} for specimens tested under the same conditions as those of the present paper [12]. These results also agree with the conclusions of Ulzurrun and Zanuy [13] for SFRC regarding the rate sensitivity of the pull-out mechanisms mobilized by straight steel fibers, showing better dynamic enhancement and lower fiber ruptures than hook-end fibers.

In RC-U55 series, the full development of the stress ribbon by the HPFRC was limited by the interface debonding, which according to the videos recorded during testing, took place very soon upon impact. Debonding can be explained by the wave sequence sketched in Figure 7c: upon impact, a compressive wave propagates firstly from the top to the bottom of the beam at midspan. Thereafter, a tensile wave is reflected and, in case a weak layer is crossed by the reflected wave, debonding can occur. According to test results, the interface between old concrete and HPFRC was able to resist the reflected wave in RC-U35 series but not in RC-U55 series. It is apparent that, for RC-U55 series, the presence of longitudinal reinforcement has weakened the interface which was unable to resist the reflected wave. This result can be explained by the reduced contact area between old concrete

and HPFRC due to the presence of the steel bars; according to the dimensions of the beam (width of 125 mm) and the diameter of the steel bars (2 × 16 mm), the contact area at the interface of RC-U55 series was 26% smaller than that of RC-U35 series.

3.2. Load-Deflection Diagrams and Energy Absorption

The two stages of tests described in Section 3.1, related to type I and II cracks, respectively, can be associated to the two stages of the total reaction-midspan deflection diagrams of Figure 6 (hereafter, referred to as load-deflection diagrams). The main characteristics of load-deflection diagrams are listed in Table 2. In addition, the maximum and residual deflections, and the energies absorbed in the two stages of tests are plotted in Figure 8a,b. The first stage of load-deflection diagrams was similar for all tested series, which is explained by the local response upon impact and the formation of type I cracks in all tests. This agrees with the similar average peak load (R_{max}) and energy absorbed in the first stage (E_1, calculated as the area below the load-deflection diagram in the first stage) shown in all series. The second stage of load-deflection diagrams is associated to the global response of the beams, the formation of type II cracks, and the activation of the stress ribbon mechanism in strengthened beams. From Figure 8b, the energy E_2 (calculated as the area below the load-deflection diagram in the second stage) absorbed by strengthened specimens was significantly larger than unstrengthened beams. On average, the increase of absorbed energy E_2 of RC-U35 and RC-U55 was 2.1 and 2.7 times the value of RC-U0, respectively. The capacity of the HPFRC layer to retain the damage of the specimens can also be demonstrated by the maximum midspan deflection (Figure 8a), which on average was 36% (RC-U35) and 39% (RC-U55) smaller than that of RC-U0 series, respectively.

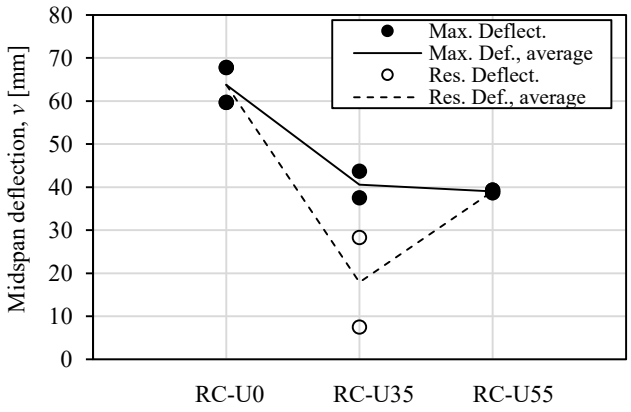

(**a**)

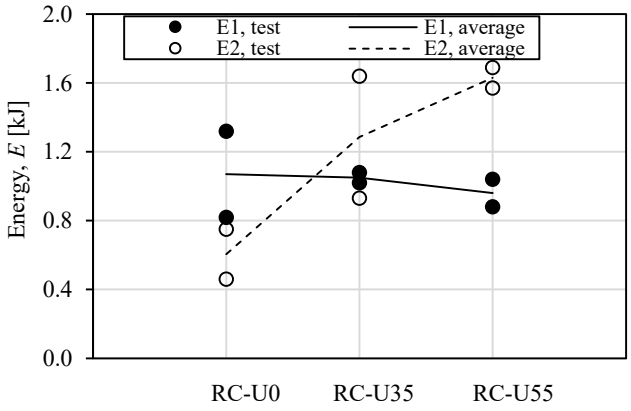

(**b**)

Figure 8. *Cont.*

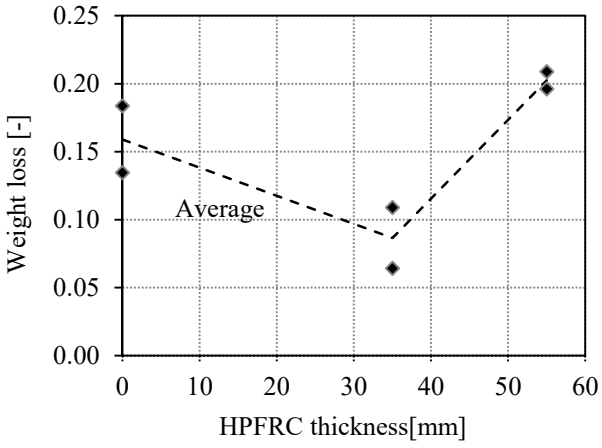

(**c**)

Figure 8. (**a**) Maximum and residual deflection; (**b**) energy absorbed in first and second stages of tests, respectively; (**c**) weight loss of specimens.

The development of interface debonding in strengthened specimens can be also analyzed with the shape of the last descending part of load-deflection diagrams (Figure 6). The integrity of the HPFRC layer in RC-U35 series corresponds with a descending part where the midspan deflection is partially recovered (i.e., the last descending branch can be seen as an unloading stage rather than a full collapse). In contrast, the last descending part of the load-deflection curves of RC-U55 series shows no deflection recovery, but sudden decrease of the load carried, which explains the spalling of the HPFRC layer. The existence of interface debonding can also be studied from the residual midspan deflection (v_{res} in Table 2, also represented in Figure 8a); it is clear that the specimens of series RC-U35 are only where the residual deflection after testing was significantly smaller than the maximum deflection.

3.3. Weight Loss and Debris

An additional indicator of impact damage is the loss of weight of the specimens due to split-out fragments. The analysis of weight loss has relevance to understand the capacity of the strengthening layer to protect goods or humans under the impacted member against induced debris. The weight loss of tested specimens is represented in Figure 8c as a function of the thickness of the HPFRC layer. It is apparent that that RC-U35 series was able to significantly reduce the generation of debris to 54% with respect to RC-U0 series. In contrast, the interfacial debonding shown by RC-U55 series was very harmful, as the generation of fragments was 28% higher than RC-U0 series due to spalling of the strengthening layer. Accordingly, it is clearly not recommended to design the strengthening layer with the interface at the same level as the longitudinal reinforcement.

3.4. Comparison with Other Configurations

In order to evaluate the capacity of the HPFRC-RC configuration to resist impact loads, a wider study was carried out by including results of previous research. Eight additional tests with identical geometry, reinforcement arrangements (concrete cover 10 mm smaller), boundary conditions, and impact load were considered from two other studies [12,22]. Among all the newly considered specimens, two were RC beams identical to series RC-U0 of this paper (only with a slightly different concrete strength, f_c = 48.5 MPa), four specimens consisted of reinforced SFRC beams (R-SFRC), and two specimens were reinforced HPFRC beams (R-HPFRC). In the R-SFRC beams, SFRC was used instead of conventional concrete. The SFRC consisted of a matrix with the same concrete as the companion RC beams and a certain amount of short straight steel fibers (l_f = 10 mm, d_f = 0.16 mm, f_y = 3000 MPa): two specimens contained 0.5% fibers by volume and two specimens 1.0%. In the R-HPFRC beams,

the conventional concrete was replaced with HPFRC with 1.6% fiber amount (l_f = 10 mm, d_f = 0.16 mm, f_y = 3000 MPa).

The RC beams presented the same impact behavior as in the present paper. The R-SFRC beams developed flexural failure with opening of a shear plug (type I cracks) in the midspan. In addition to the shear plug, type II diagonal cracks opened in the webs but the bridging capacity of the SFRC was able to avoid their propagation. The residual width of diagonal cracks and shear plugs was larger in the specimens with 0.5% fiber content than with 1.0%. The R-HPFRC developed flexural failure mode with a major bending crack at midspan and no shear cracking at all.

The results of all considered tests are represented in Figure 9 in terms of strength (maximum value of total reaction) and maximum midspan displacement produced by the impact. As it can be noted, the highest strength was obtained by the R-HPFRC beams followed by the R-SFRC beams with 1.0% fiber content and the R-SFRC with 0.5% fiber. The deformation capacity under impact can be evaluated by means of maximum deflection obtained at the midspan. From Figure 9, the average midspan deflection of HPFRC-strengthened RC specimens was 37% smaller than that of RC beams failing by brittle shear and severe fragmentation, while that of R-HPFRC specimens failing by flexure was 75% smaller than that of RC. The comparison of maximum deflection indicates that the HPFRC-RC beams showed an intermediate deformation capacity between RC and R-HPFRC. The smaller strength and higher deflection of RC-U55 with respect to RC-U35 was due to the full development of the additional resisting mechanism as stress ribbon by RC-U35 series.

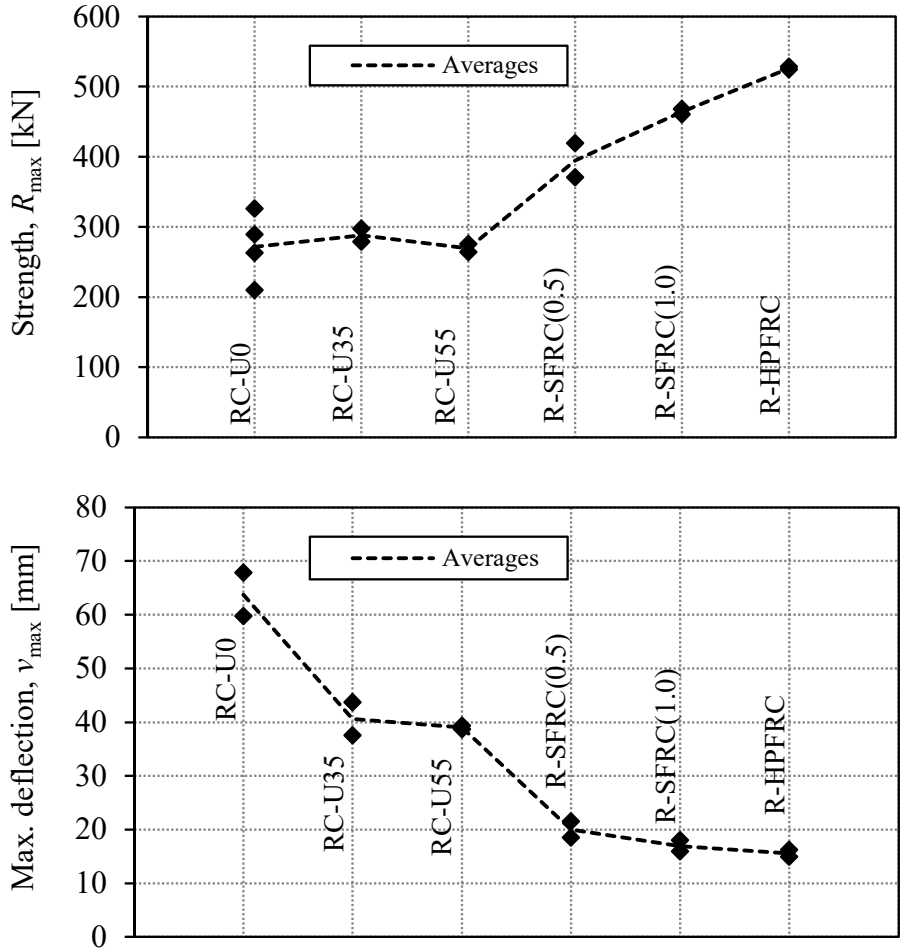

Figure 9. Comparison of results of the tests of the present paper and those from [12,22].

4. Conclusions

The results presented in this paper are intended to understand the potential of shear-critical HPFRC-RC members subjected to impacts. According to the results, the following conclusions can be drawn:

I. RC beams presented brittle shear failure with significant fragmentation. Strengthening with HPFRC reduced fragmentation but types I and II cracks also formed. The beams strengthened with HPFRC layer presented an additional resisting mechanism with the HPFRC working similarly to a stress ribbon. This additional contribution was activated in the second stage of tests characterized by global behavior. The stress ribbon mechanism provided an energy absorption in the second stage (E_2) 2.1 and 2.7 times that of the unstrengthened beams, in the case of specimens with 35 mm and 55 mm strengthening layers, respectively.

II. Interface debonding can occur when the tensile reflected wave induced by the impact crosses the interface between concretes, as observed in the last stage of impact tests of RC-U55 series. In such series, the interface was placed at the level of the longitudinal reinforcement, which reduced the contact surface between concretes and weakened the impact behavior. Accordingly, it is recommended to avoid such design configuration.

III. In comparison with results from previous research of R-HPFRC and R-SFRC beams failing by flexure under impact, HPFRC-RC presents an intermediate behavior between them and conventional RC in terms of strength and deformation capacity.

IV. Strengthening with HPFRC tensile layer presents interesting potential for existing RC structures as a new resisting mechanism provided by the HPFRC working similarly as a stress ribbon can reduce impact debris, thereby protecting humans and goods below the structure. Future research is still needed in order to quantify the contribution of the new resisting mechanism.

V. The research presented in this paper has shown that a structural solution for existing shear-critical RC members susceptible to suffer impacts can be based on the application of a thin HPFRC layer on the tensile side. In order to achieve the stress ribbon mechanism found for this structural solution, structural designers are recommended to consider the following guides:

    a. A fiber amount of at least 2% for the HPFRC to achieve strain hardening.
    b. The interface between the old concrete and the HPFRC should not be placed at the level of the longitudinal reinforcement.
    c. A surface preparation of the old concrete with hydro-jetting or sand-blasting before application of the HPFRC is recommended. In case the tensile side is at the bottom, a prefabricated HPFRC laminate can be alternatively bonded with epoxy adhesive.

Notations

E_1	energy absorbed in the first stage
E_2	energy absorbed in the second stage
E_{CU}	elastic modulus of HPFRC
G_F	fracture energy
$R_{\max}$	peak total reaction
d_f	diameter of steel fibers
f_c	concrete compressive strength

f_{CU}	compressive strength of HPFRC
f_y	yield strength of steel fibers
l_f	length of steel fibers
v	deflection at midspan
v_{max}	peak deflection at midspan
v_{res}	residual deflection at midspan
w	crack width
ε_{pc}	hardening strain at peak strength of HPFRC
ρ	steel reinforcing ratio
σ_{cc}	matrix cracking strength of HPFRC
σ_{pc}	peak strength of HPFRC

Author Contributions: Formal analysis, C.Z. and G.S.D.U.; investigation, C.Z. and G.S.D.U.; writing—original draft, C.Z.; writing—review and editing, C.Z. All authors have contributed to the whole paper. All authors have read and agreed to the published version of the manuscript.

Funding: This research was funded by the Spanish Agency for Research (Project ID BIA2016-74960-R AEI/FEDER, UE).

Acknowledgments: The CRC pre-mix and fibers were kindly provided by Hi-Con A/S (Denmark). Thanks to "Fundación José Entrecanales Ibarra" for funding the PhD fellowship of the second author.

Conflicts of Interest: The authors declare no conflicts of interest.

References

1. Habel, K.; Gauvreau, P. Behavior of reinforced and posttensioned concrete members with a UHPFRC overlay under impact loading. *J. Struct. Eng.* **2009**, *135*, 292–300. [CrossRef]
2. Qiu, J.; Wu, X.G.; Jiang, H. Influences of rehabilitation material parameter on existing PC parapets. In Proceedings of the 2015 World Congress on Advances in Structural Engineering and Mechanics (ASEM15), Incheon, Korea, 25–29 August 2015; Techno-Press: Daejeon, Korea, 2015; pp. 1–14.
3. Qiu, J.; Wu, X.G.; Hu, Q. Crashworthiness analysis on existing RC parapets rehabilitated with UHPCC. *Comp. Concr.* **2017**, *19*, 87–98. [CrossRef]
4. Hrynyk, T.D.; Vecchio, F.J. Behavior of steel fiber-reinforced concrete slabs under impact load. *ACI Struct. J.* **2014**, *111*, 1213–1223. [CrossRef]
5. Micallef, K.; Sagaseta, J.; Fernández Ruiz, M.; Muttoni, A. Assesssing punching shear failure in reinforced concrete flat slabs subjected to localised impact loading. *Int. J. Impact Eng.* **2014**, *71*, 17–33. [CrossRef]
6. Saatci, S. Behaviour and Modelling of Reinforced Concrete Structures Subjected to Impact Loads. Ph.D. Thesis, University of Toronto, Toronto, ON, Canada, 2007.
7. Kishi, K.H.; Mikami, H.; Matsuoka, K.G.; Ando, T. Impact behavior of shear-failure type RC beams without shear rebar. *Int. J. Impact Eng.* **2002**, *27*, 955–968. [CrossRef]
8. Yi, W.J.; Zhao, D.B.; Kunnath, S.K. Simplified approach for assessing shear resistance of reinforced concrete beams under impact loads. *ACI Struct. J.* **2016**, *113*, 747–756. [CrossRef]
9. Adhikary, S.D.; Li, B.; Fujikake, K. Dynamic behavior of reinforced concrete beams under varying rates of concentrated loading. *Int. J. Impact Eng.* **2012**, *47*, 24–38. [CrossRef]
10. Pham, T.M.; Hao, H. Plastic hinges and inertia forces in RC beams under impact loads. *Int. J. Impact Eng.* **2017**, *103*, 1–11. [CrossRef]
11. Schellenberg, K. On the Desing of Rockfall Protection Galleries. Ph.D. Thesis, ETHZ Swiss Federal Institute for Technology, Zurich, Switzerland, 2008.
12. Ulzurrun, G.; Zanuy, C. Enhancement of impact performance of reinforced concrete beams without stirrups by adding steel fibers. *Con. Build Mat.* **2017**, *145*, 166–182. [CrossRef]
13. Ulzurrun, G.; Zanuy, C. Flexural response of SFRC under impact loading. *Con. Build Mat.* **2017**, *134*, 397–411. [CrossRef]
14. Tran, T.K.; Kim, D.J. High strain rate effects on direct tensile behaviour of high performance fiber reinforced cementitious composites. *Cem. Concr. Comp.* **2014**, *45*, 186–200. [CrossRef]
15. Zhang, X.; Ruiz, G.; Tarifa, M.; Cendón, D.; Gálvez, F.; Alhazmi, W.H. Dynamic fracture behavior of steel fiber reinforced self-compacting concretes (SFRSCCs). *Materials* **2017**, *10*, 1270. [CrossRef] [PubMed]

16. Mechtcherine, V.; Silva, F.A.; Butler, M.; Zhu, D.; Mobasher, B.; Gao, S.L.; Mäder, E. Behaviour of strain-hardening cement-based composites under high strain rates. *J. Adv. Concrete. Tech.* **2011**, *9*, 51–62. [CrossRef]
17. Chorzepa, M.G.; Masud, M.; Yaghoobi, A.; Jiang, H. Impact test: Multiscale fiber-reinforced concrete including polypropilene and steel fibers. *ACI Mat. J.* **2017**, *114*, 1429–1444. [CrossRef]
18. American Concrete Institute. *Ultra-High-Performance Concrete: An Emerging Technology Report*; ACI 239R-18; American Concrete Institute: Farmington Hills, MI, USA, 2018.
19. AFGC. *Ultrahigh Performance Fiber Reinforced Concretes. Recommendations*; AFNOR: Paris, France, 2002.
20. SIA. *SIA 2052. Ultra-Hochleistungs-Faserbeton (UHFB) Baustoffe, Bemessung und Ausführung*; Swiss Engineers and Architects: Bern, Switzerland, 2016.
21. Habel, K.; Viviani, M.; Denairé, E.; Brühwiler, E. Development of the mechanical properties of an ultra-high performance fiber reinforced concrete (UHPFRC). *Cem. Concr. Res.* **2006**, *36*, 1362–1370. [CrossRef]
22. Zanuy, C.; Ulzurrun, G. Impact performance of low-fiber content HPFRCC: From material to structural behavior. In Proceedings of the International Conference Strain-hardening Cement-based Composites (SHCC 4), Dresden, Germany, 18–20 September 2017; RILEM Proceeding-Springer: Berlin, Germany, 2017; pp. 473–481.
23. Yoo, D.Y.; Banthia, N.; Kim, S.W.; Yoon, Y.S. Response of ultra-high-performance fiber-reinforced concrete beams with continuous steel reinforcement subjected to low-velocity impact loading. *Comp. Struct.* **2015**, *126*, 233–245. [CrossRef]
24. Othman, H.; Marzouk, H. Impact response of ultra-high-performance reinforced concrete plates. *ACI Struct. J.* **2016**, *113*, 1325–1334. [CrossRef]
25. Wille, K.; Kim, D.J.; Naaman, A.E. Strain-hardening UHP-FRC with low fiber contents. *Mat. Struct.* **2011**, *44*, 583–598. [CrossRef]
26. Habel, K.; Denairé, E.; Brühwiler, E. Structural response of elements combining ultrahigh-preformance fiber-reinforced concretes and reinforced concrete. *J. Struct. Eng.* **2006**, *132*, 1793–1800. [CrossRef]
27. Noshiravani, T.; Brühwiler, E. Experimental investigation on ultra-high-preformance fiber-reinforced concrete composite beams subjected to combined bending and shear. *ACI Struct. J.* **2013**, *110*, 251–261.
28. Pimentel, M.; Nunes, S. Experimental tests on RC beams reinforced with a UHPFRC layer failing in bending and shear. In Proceedings of the 4th International Symposium on Ultra-High Performance Concrete and High Performance Materials, Kassel, Germany, 9–11 March 2016; University of Kassel: Kassel, Germany, 2016; pp. 1–9.
29. Noshiravani, T.; Brühwiler, E. Analytical model for predicting response and flexure-shear resistance of composite beams combining reinforced ultrahigh performance fiber-reinforced concrete and reinforced concrete. *J. Struct. Eng.* **2014**, *140*, 1–10. [CrossRef]
30. Tran, N.T.; Tran, T.K.; Jeon, J.K.; Park, J.K.; Kim, D.J. Fracture energy of ultra-high-performance fiber-reinforced concrete at high strain rates. *Cem. Concrete Res.* **2016**, *79*, 169–184. [CrossRef]
31. Tran, N.T.; Tran, T.K.; Kim, D.J. High rate response of ultra-high-performance fiber-reinforced concretes under direct tension. *Cem. Concrete Res.* **2015**, *69*, 72–87. [CrossRef]
32. Pyo, S. Characteristics of Ultra High Performance Concrete Subjected to Dynamic Loading. Ph.D. Thesis, University of Michigan, Ann Arbor, MI, USA, 2014.
33. Kim, J.H.; Kim, D.; Han, H.N.; Barlat, F.; Lee, M.G. Strain rate dependent tensile behaviour of advanced high strength steels: Experiments and constitutive modelling. *Mat. Sci. Eng. A* **2013**, *559*, 222–231. [CrossRef]
34. Kim, D.J. Strain Rate Effect on High Performance Fiber Reinforced Cementitious Composites Using Slip Hardening High Strength Deformed Steel Fibers. Ph.D. Thesis, University of Michigan, Ann Arbor, MI, USA, 2009.
35. Habel, K.; Gauvreau, P. Response of ultra-high performance fiber reinforced concrete (UHPFRC) to impact and static loading. *Cem. Concr. Comp.* **2008**, *30*, 938–946. [CrossRef]
36. Bindiganavile, V.; Banthia, N.; Aarup, B. Impact response of ultra-high-strength fiber-reinforced cement composite. *ACI Mat. J.* **2002**, *99*, 543–548.
37. Soleimani, S.M.; Banthia, N. A novel drop weight impact setup for testing reinforced concrete beams. *Exp. Tech.* **2012**, *38*, 1–8. [CrossRef]
38. International Federation for Structural Concrete (FIB). *Bulletin No. 85. Towards a Rational Understanding of Shear in Beams and Slabs*; FIB: Lausanne, Switzerland, 2018; 338p.
39. Tanarslan, H.M.; Alver, N.; Jahangiri, R.; Yalcinkaya, C.; Yazici, H. Flexural strengthening of RC beams using UHPFRC laminates: Bonding techniques and rebar addition. *Constr. Build Mat.* **2017**, *155*, 45–55. [CrossRef]

40. Al-Osta, M.A.; Isa, M.; Baluch, M.H.; Rahman, M.K. Flexural behavior of reinforced concrete beams strengthened with ultra-high performance fiber reinforced concrete. *Constr. Build Mat.* **2017**, *134*, 279–296. [CrossRef]
41. López, J.A.; Serna, P.; Navarro-Gregori, J.; Coll, H. A simplified five-point inverse analysis method to determine the tensile properties of UHPFRC from unnotched four-point bending tests. *Comp. Part B* **2016**, *91*, 189–214. [CrossRef]
42. Zhang, X.X.; Ruiz, G.; Yu, R.C.; Tarifa, M. Fracture behaviour of high-strength concrete at wide range of loading rates. *Int. J. Impact Eng.* **2009**, *36*, 1204–1209. [CrossRef]
43. Banthia, N.; Yan, C.; Sakai, K. Impact resistance of fiber reinforced concrete at subnormal temperatures. *Cem. Concr. Comp.* **1998**, *20*, 393–404. [CrossRef]
44. Zhang, X.X.; Abdelazim, A.M.; Ruiz, G.; Yu, R.C. Fracture behaviour of steel fibre-reinforced concrete at a wide range of loading rates. *Int. J. Impact Eng.* **2014**, *71*, 89–96. [CrossRef]
45. Ong, K.C.G.; Basheerkhan, M.; Paramasivam, P. Resistance of fibre concrete slabs to low velocity projectile impact. *Cem. Concr. Comp.* **1999**, *21*, 391–401. [CrossRef]
46. Bastien Masse, M.; Brühwiler, E. Contribution of R-UHPFRC strengthening layers to the shear resistance of RC elements. In Proceedings of the 4th International Symposium on Ultra-High Performance Concrete and High Performance Materials, Kassel, Germany, 9–11 March 2016; University of Kassel: Kassel, Germany, 2016; pp. 127–128.
47. Li, H.L.; Chen, W.; Hao, H. Dynamic response of precast concrete beam with wet connection subjected to impact loads. *Eng. Struct.* **2019**, *191*, 247–263. [CrossRef]